Control Engineering Practice 86 (2019) 166–174

Contents lists available at ScienceDirect

Control Engineering Practice

journal homepage: www.elsevier.com/locate/conengprac

Concurrent design of controller and passive elements for robots with impulsive actuation systems

Rezvan Nasiri [a,*], Armin Zare [a], Omid Mohseni [a], Mohammad Javad Yazdanpanah [b], Majid Nili Ahmadabadi [a,1]

[a] Cognitive Systems Laboratory, Control and Intelligent Processing Center of Excellence (CIPCE) School of Electrical and Computer Engineering, College of Engineering, University of Tehran, Iran

[b] Advanced Control Systems Laboratory, Control and Intelligent Processing Center of Excellence (CIPCE) School of Electrical and Computer Engineering, College of Engineering, University of Tehran, Iran

ARTICLE INFO

Keywords:
Impulsive actuation
Bio-inspired control
Legged robot
Compliance and damper design
Cyclic task
Explosive task

ABSTRACT

There are some biological evidences showing that the actuation system in legged animals is impulsive; it is not continuous. As opposed to continuous control/actuation, the control actions occur in specific intervals, and from the instant of one actuation until the start of the next one, passive elements guarantee the stability of the robotic system and govern its natural dynamics. In this paper, we present an analytical method for concurrent design of impulsive controller and passive elements (compliance and damper) for robotic systems; e.g., manipulators and legged-robots. To optimize the force profiles of passive elements, three different cost functions are presented which optimize the natural dynamics and energy consumption of the robot. The presented method can be applied to both cyclic and non-cyclic (explosive) tasks so as to attain energy efficient and bio-inspired motions. The method is applied to three biological models: a simulated human arm for throwing an object, a swing leg for drawing an oval, and a 3D quadruped robot for performing walking gait. Our findings in the simulation studies are in line with the hypothesis of impulsive actuation in nature and show the applicability of our method in robotics.

1. Introduction

Wilson, Watson, and Lichtwark (2003) showed that large cursorial animals, such as horses, rely on a catapult mechanism for rapid acceleration and preparing for the next stance phase. It implies, in contrast to a mass–spring model, energy is stored slowly and then released in a very short period of time; i.e., in nature, we may have an impulsive/discontinuous actuation system along with a compliant body.

Biological systems mainly perform cyclic tasks by benefiting from the natural dynamics of their magnificent compliant structure; see Biewener and Roberts (2000) and Dickinson et al. (2000). Accordingly, for the sake of efficiency, they mostly consume energy whenever their body deviates from the desired motion. For instance, it has been shown that in walking, energy is inserted just after the impact moment by push-off, and the interval between the toe-off and the heel-strike is traversed largely passively (Caputo & Collins, 2014; Meinders, Gitter, & Czerniecki, 1998; Srinivasan & Ruina, 2006; Zamani & Bhounsule, 2017; Zelik, Huang, Adamczyk, & Kuo, 2014). More specifically, during the pre-swing sub-phase of gait, one exerts a comparatively large torque at the ankle joint to properly push-off and traverse the swing phase. Interestingly, researchers motivated by this fact employed a similar approach in controlling bipedal robots on level ground walking; see Aoustin, Romero, Chevallereau, and Aubin (2006), Byl and Tedrake (2008), Choi and Grizzle (2005), Collins, Ruina, Tedrake, and Wisse (2005) and Formalskii (2009). Moreover, recently, impulsive control is also practiced in some specific robotic systems; see Bhounsule, Ruina, and Stiesberg (2015), Giardina and Iida (2018), Haldane, Plecnik, Yim, and Fearing (2016) and Mathis, Jafari, and Mukherjee (2014). These very evidences provided an incentive for us to present a general mathematical framework for using impulsive actuation instead of continuous actuation, which is restricted to a finite set of discrete actuation points so as to accomplish a task of continuous nature with minimum actuation intervals.

From control systems point of view, not all continuous tracking problems require continuous control; some only might need certain goals to be met at distinct points along the trajectory. In other words,

* Corresponding author.
E-mail addresses: nasiri.rezvan@gmail.com (R. Nasiri), armin.zare1991@gmail.com (A. Zare), o.mohseni.sh@gmail.com (O. Mohseni), yazdan@ut.ac.ir (M.J. Yazdanpanah), mnili@ut.ac.ir (M.N. Ahmadabadi).
[1] Principal Investigator (PI).

https://doi.org/10.1016/j.conengprac.2019.03.014
Received 20 July 2018; Received in revised form 21 March 2019; Accepted 22 March 2019
Available online 3 April 2019
0967-0661/

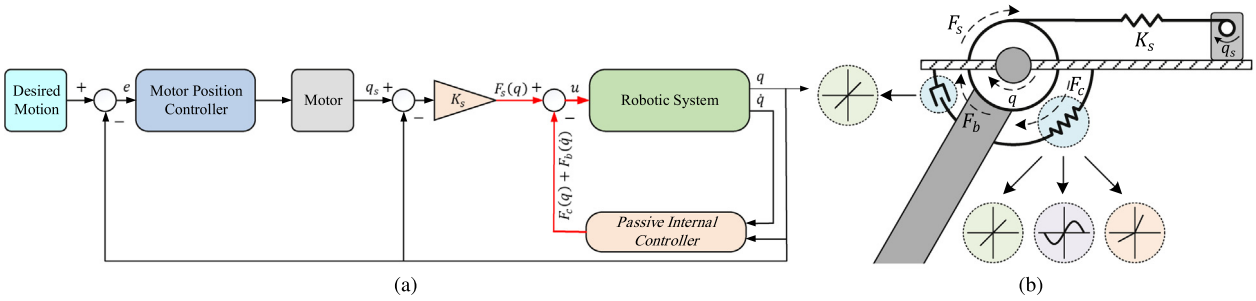

Fig. 1. Schematics of the presented method from two different perspectives. (a) Block diagram of the presented control loop. (b) Realization of the impulsive actuation, compliance, and damper forces.

a tracking task can turned into some regulation subtasks which subsequently could be fulfilled with discrete control laws instead of continuous control. However, two issues must be taken care of for this control strategy to work: **(1)** it is essential to guarantee reaching to regulation set points, and **(2)** the trajectory between two subsequent set points must be that of interest. Needless to say, now that our only influence on the system is in short intervals, satisfying these two objectives at the same time pertains solely to natural dynamics of the system. This means that, the natural dynamics (unforced dynamics) of the system plays the key role in the intervals when there is no control present. To make sure that the behavior of the system in these intervals satisfies the need of the desired task, partial modification of the structure (Natural Dynamics Modification, NDM in short, see Khoramshahi, Parsa, Ijspeert, & Nili Ahmadabadi, 2014) in most cases is required. NDM techniques incorporate passive elements (i.e., compliance and damper) in the robot's structure and they have been employed in many previous works both offline (Plooij & Wisse, 2012; Shushtari, Nasiri, Yazdanpanah, & Ahmadabadi, 2017; Verstraten et al., 2016) and online (Nasiri, Khoramshahi, Shushtari, & Ahmadabadi, 2016).

What we present in this work is a bio-inspired approach for control of compliant systems with impulsive actuations, which provides an analytical framework for a new concept in actuation systems; impulsive elastic actuators (von Brecht, Kramer, Bhounsule, & Jafari, 2016). By means of this method, the system is able to move along its desired trajectory largely passive with the aid of properly added compliances and dampers in its structure and finite control actions occurring at certain points. We prove that through the use of these passive elements in an n-DOF manipulator, the dynamical equations become stable and convergent to any desired configuration. The proposed method can be used both for explosive and cyclic tasks.

The rest of the paper is organized as follows: The problem is stated in Section 2. Section 3 focuses on the mathematical analysis of the proposed method. Section 4 presents three simulation studies, and conclusions are drawn in the last section.

2. Problem statement

Consider the dynamical equations of a general n-DOF manipulator system as

$$M(q)\ddot{q} + C(q,\dot{q})\dot{q} + G(q) = u \tag{1}$$

where $u \in \mathbb{R}^n$ is the vector of input torques (or forces), and $q, \dot{q}, \ddot{q} \in \mathbb{R}^n$ are the vectors of joint positions, velocities and accelerations, respectively. $M(q) \in \mathbb{R}^{n\times n}$ is the positive-definite mass-inertia matrix, $C(q,\dot{q}) \in \mathbb{R}^{n\times n}$ is the matrix of centrifugal and Coriolis terms, and $G(q) \in \mathbb{R}^n$ is the vector of terms associated with conservative potentials.

According to Wilson et al. (2003), the muscle extension/flexion force is in linear relation with its displacement. Moreover, ligaments can be modeled as nonlinear parallel compliances in robotic systems. In addition, as it is studied in Hill (1938), the muscle force is in monotonic relation with its velocity. Therefore, a simplified formulation of the muscle function is presented as:

$$u = -F_s(q) - F_c(q) - F_b(\dot{q}) \;;\; F_s(q) = K_s(q - q_s) \tag{2}$$

where $F_c(q) \in \mathbb{R}^n$ and $F_b(\dot{q}) \in \mathbb{R}^n$ are the vectors of parallel nonlinear compliance and damper forces, respectively. $F_s(q) \in \mathbb{R}^n$ is the vector of series linear spring forces, $K_s \in \mathbb{R}^{n\times n}$ is the diagonal matrix of stiffnesses for series springs, and the q_s vector is the control parameter corresponding to series springs' rest lengths; see Fig. 1. We aim at achieving the given/desired task by regulating this parameter (q_s) at actuation intervals. By means of this mathematical definition for the input (u), the compliance and damper forces play the role of a *Passive Internal Controller* (PIC) which stabilizes the system between two consecutive actuation intervals. Fig. 1a presents a schematic of the proposed controller. According to Fig. 1a, u could be regarded as a combination of a nonlinear state feedback ($F_c(q) + F_b(\dot{q})$) and a semi-active actuation ($K_s(q - q_s)$). The realization of this control block diagram can be illustrated as in Fig. 1b. We name this combination of PIC and semi-active actuations as an *Impulsive Actuation System* (IAS).

Definition 1 (*Compliance and Damper Forces*)**.** F_c and F_b in the jth joint are defined as

$$f_{cj}(q_j) = \sum_{i=1}^{m} k_{ij}\phi_{ij} = K_j^T \boldsymbol{\Phi}_j(q_j) \quad , \quad K_j, \boldsymbol{\Phi}_j \in \mathbb{R}^m \tag{3}$$

$$f_{bj}(\dot{q}_j) = \sum_{i=1}^{m} b_{ij}\psi_{ij} = B_j^T \boldsymbol{\Psi}_j(\dot{q}_j) \quad , \quad B_j, \boldsymbol{\Psi}_j \in \mathbb{R}^m \tag{4}$$

where ϕ_{ij} and ψ_{ij} are the ith basis function for compliance and damper, respectively. Also k_{ij} and b_{ij} represent their coefficients in the order given.

This definition could represent any type of compliance and damper force profiles provided that the basis functions (ϕ_{ij} and ψ_{ij}) are chosen properly. Although there is no obstacle in implementing nonlinear compliances (Bidgoly, Ahmadabadi, & Zakerzadeh, 2016; Kim & Deshpande, 2014), still no general method for implementation of nonlinear dampers is put forward. Hence, for the sake of implementation constraints, in simulations, we only consider a linear basis for damper forces and assume the passivity condition as follows.

Assumption 1 (*Passivity Condition*)**.** F_b in the jth joint should satisfy the following inequality.

$$b_{ij} > 0 \quad , \quad \forall i, j \tag{5}$$

Hereinafter, we merge the $K_s q$ term in $F_s(q)$ with $F_c(q)$ and redefine the rest as $F_d = K_s q_s$, which in fact corresponds to the precompression of the springs.

$$u = F_d - F_c(q) - F_b(\dot{q}) \;\; ; \;\; F_d = K_s q_s \tag{6}$$

Based on this new definition of u, one can easily check that the definitions of F_c and F_b in Eqs. (3) and (4) still hold. However, merging

$K_s q$ with $F_c(q)$ necessitates having a linear basis function in each joint; i.e., $\phi_{1j} = q_j$.

In this paper, the goal is to design IAS described in Eq. (2) in such a way that the desired task is done efficiently; i.e., with minimum number of actuation intervals per each cycle. In doing so, we divide each cycle to some discontinuous motions (explosive tasks or subtasks), and by means of the PIC design ($F_c(q)$ and $F_b(\dot{q})$), the robot passively performs the subtasks. Once the system reaches to the end of each subtask, F_d is changed (by controlling q_s) in a short interval, and it triggers another subtask. Then by chaining these subtasks, the main task is born; see Fig. 2. The PIC between two consecutive intervals (in absence of F_d variations) should guarantee **(1)** the dynamical stability of the system and **(2)** the convergence towards the next actuation interval.

3. Mathematical analysis

In this section, first we consider only an arbitrary subtask of a cyclic task, and determine the stability conditions for PIC (F_c and F_b) in order to perform the considered subtask. Here, performing a subtask means converging to a vicinity of equilibrium point in each subtask where the next subtask is started. Thereafter, we address the issue of how this method could be developed for having a cyclic task.

3.1. Stability analysis

In order to show that the use of compliance and damper forces (Eqs. (3) and (4)) is adequate for stabilizing the system described in Eq. (1), first we rewrite the dynamical equations of the system by substituting Eq. (6) into Eq. (1).

$$H^*(q,\dot{q},\ddot{q}) = M(q)\ddot{q} + C(q,\dot{q})\dot{q} + G(q) + F_c(q) + F_b(\dot{q}) - F_d = 0 \tag{7}$$

To show that the control law stated in Eq. (6) stabilizes the system, consider the following storage function

$$V = T(q,\dot{q}) + U(q) + \int_{q_e}^{q} \left(F_c(z) - F_d\right) dz, \quad F_c\left(q_e\right) = F_d \tag{8}$$

where the first two terms represent the kinetic energy and potential energy caused by gravity, respectively. In addition, the third term is potential energy stored in the compliance. Computing the time derivative of Eq. (8) results in $\dot{V} = -\dot{q}^T F_b(\dot{q})$, which according to Eqs. (4) and (5) is n.s.d. Therefore, based on the "*Passivity Theorem*" (Khalil, 2002, pp. 444), it is deduced that the system is asymptotically stable. Now the next step is to determine the equilibrium point to which the system converges.

3.2. Determining the equilibrium point

From the stability proof in Section 3.1, it can be inferred that, in each subtask not only Eq. (6) stabilizes the system, but also provides us with more freedom to design the desired equilibrium point. By defining the desired equilibrium point (at the end of each subtask) as: $\Theta \triangleq \{q_d \ , \ \ddot{q_d} = \dot{q_d} = 0\}$, and substituting it into Eq. (7), we obtain:

$$F_d = G(q_d) + F_c(q_d) \tag{9}$$

It means that, for reaching to the desired equilibrium point, F_d must satisfy Eq. (9). However, since the dynamical equations of the robot (Eq. (1)) are highly nonlinear, Eq. (9) is not a sufficient condition for the existence of an asymptotically stable equilibrium point and it is just a necessary condition. Based on the mathematics presented in Ott (2008), if the compliance force at the jth joint satisfies the following condition, then (in each subtask) the robot reaches the desired equilibrium point.

$$\forall q \in \mathbb{Q} \subset \mathbb{R}^n \ , \ \exists \alpha > 0 \rightarrow \left\| \frac{\partial G(q)}{\partial q} \right\|_2 < \alpha \tag{10}$$

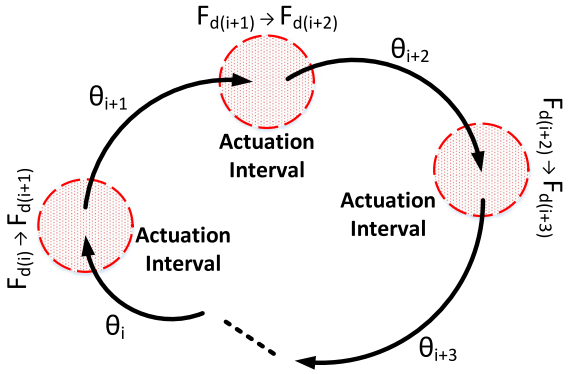

Fig. 2. Discretization of a cyclic task. Dividing a periodic path into some arbitrary subtasks results in a number of aperiodic paths. Thereafter, the controller should provide condition for transition from one subtask (Θ_i) to the next one (Θ_{i+1}). According to Eq. (9), to trigger a new subtask, we need to change $F_{d(i)}$ to $F_{d(i+1)}$. The key thing to notice is that, this transition must be done smoothly so that it does not deteriorate the performance of robot. Therefore, a vicinity of some radius is considered for the controller to act. Red circles centered at the transition phases represent such vicinities; i.e., control/actuation interval.

$$f_{ci} q_i > \alpha q_i^2 \quad ; \quad i = 1, \ldots, n \tag{11}$$

In this equation, $\mathbb{Q}$ is the feasible trajectory space of the robot which is a subset of $\mathbb{R}^n$. The compliance force should satisfy Eq. (11) which implies that the compliance forces should be sufficiently high to prevent the manipulator to fall down by the effect of gravity; i.e., it is a bifurcation condition. In order to satisfy this condition, it is sufficient to have a linear basis ($\phi_{1j} = q_j$) with positive coefficient ($k_{1j} \geq \alpha$) in the compliance force (Eq. (4)).

3.3. Cyclic tasks

Up to here, using the method presented earlier, one can move the robot from the start condition to the equilibrium point in each subtask passively. In fact, for performing each subtask or a certain explosive task, our method does not need any actuation at all; just initialize the robot and it will converge to the desired equilibrium point and the explosive task is done. But this approach may seem improper for cyclic tasks at the first glance. Here, we propose a simple control strategy to extend our previous approach for periodic motions.

For a given reference cyclic path, one can split the path into some arbitrary subtasks (N_d)[2] (resulting in several aperiodic paths) and subsequently apply the preceding method for each. Since according to our method, moving from one configuration to another is done stably and with no controller present, we do not need any controller along the way. The only control required is when the robot approaches to a vicinity near to desired equilibrium point in each subtask. Hence, in each subtask, to perform a smooth and energy efficient cyclic task, we do not let the robot to halt at equilibrium point and apply the *impulsive actuation* before this instance.

In order for this work to be done, whenever the robot approaches a vicinity near to the equilibrium point in each subtask, the controller must provide the system with new F_d to trigger another subtask; see Fig. 2 for more details. As illustrated in this figure, for proceeding from Θ_i to Θ_{i+1}, the controller must supply the system with $F_{d(i+1)}$ if the tracking error ($e(t) = q_d(t) - q(t)$) at transition phases ($t = t_{TP}$) is higher than a decision boundary ($|e(t_{TP})| > \epsilon$). Accordingly, the number of

[2] N_d is the number of subtasks and can be intuitively chosen based on the application. For instance, inspired from the biological evidences of human walking at toe-off, it can be deduced that for a legged robot to walk stably and possibly efficient, a push off right before the swing phase might be required. Thus, *impulsive actuation* at this very instance is recommended (see Kuo (2002) and McGeer (1993)).

impulsive actuations (N_r) is either $N_r < N_d$ or $N_r = N_d$. This in turn guarantees approaching towards Θ_{i+2} stably. In fact, according to Eq. (6), this act of supplying the system with $F_{d(i)}(i = 1, 2, ..)$ at certain intervals is equivalent to setting the rest length of series spring (q_s).

It must be noted that there is no need for changing the coefficients of compliances and dampers in each subtask, since for moving stably from one configuration to another, only Eqs. (5), (9), and (11) must be held. Among these three equations, Eqs. (5) and (11) are inequalities which are easier to satisfy. This point indicates the robustness of the presented method while the stability is guaranteed under a minor constraint.

3.4. Damper and compliance optimization

In previous subsections, we stated some constraints on compliance and damper forces ($F_c(q)$ and $F_b(\dot{q})$) in order to guarantee convergence to the desired equilibrium point. However, choosing the coefficients that satisfy these constraints, only guarantees convergence and there is no control over the trajectory towards the equilibrium point. Except Eq. (9), all the other constraints are inequalities which cannot determine the coefficients of passive elements directly; i.e., we have a redundancy between constraints and free parameters. Using this redundancy, one can determine a desired trajectory or improve energy efficiency. To this end, an optimization approach is suggested as:

$$\begin{aligned} &\left(K_{opt}, B_{opt}\right) = arg\min_{K,B} J(K, B) \\ &s.t. \begin{cases} F_d = G(q_d) + F_c(q_d) \\ b_{ij} > 0 \quad , \quad \forall i, j \\ f_{ci} q_i > \alpha_i q_i^2 \quad , \quad q_i \neq 0 \end{cases} \\ &K = \left[K_1{}^T K_2{}^T \cdots K_n{}^T\right]^T \ , \ B = \left[B_1{}^T B_2{}^T \cdots B_n{}^T\right]^T \end{aligned} \tag{12}$$

where $J(K, B)$ is a cost function which can take different forms depending on the application. It is important to note that the number of subtasks and timing of actuation intervals can also be considered as free parameters for optimization. However, for the sake of simplicity, in this optimization problem, they are fixed and predefined functions of time.

Here, we present three different cost functions each aiming to optimize a specific characteristic of the system; e.g., tracking error or energy efficiency.

$$J_1 = \int_0^T H_r^{*T} H_r^* dt \tag{13}$$

$$J_2 = \int_0^T \beta(t)(q_r - q)^2 + \lambda(t)(\dot{q}_r - \dot{q})^2 dt \tag{14}$$

$$J_3 = E_c/(m_t g d) \tag{15}$$

where in Eq. (13), $H_r^* = H^*(q_r, \dot{q}_r, \ddot{q}_r)$ with q_r being the reference trajectory. This cost function aims at increasing the consistency of the dynamical equations of the robot with the reference trajectory. Accordingly, $H_r^* \equiv 0$ means that the reference trajectory (q_r) is completely consistent with the dynamical equations of the robot (Eq. (7)) and the robot can passively move over q_r; i.e., q_r is the time response of Eq. (7). Unlike the first cost function that tries to increase the consistency between the reference and real trajectories from a dynamical point of view, the second cost function (Eq. (14)) directly targets the kinematic similarity between them. In Eq. (14), $\lambda(t)$ and $\beta(t)$ are arbitrary time-dependent weights. Since the closed form time response of the nonlinear dynamical equations (as robots) cannot be computed in general, to minimize Eq. (14), it is recommended to employ a non-classic optimization algorithm; e.g., genetic algorithm (GA). Compared to Eq. (14), the computation of Eq. (13) seems to be more complicated and needs dynamical equations of the robot, however, in some cases, it can be analytically solved.

In Eq. (15) we minimize the cost of transportation (COT) of legged robots. In Eq. (15), E_c is the total energy consumption which is the summation of injected energies at actuation intervals; see Section 3.5 for E_c computation. Moreover, m_t is the total mass of the legged robot, and d is the locomotion distance. By minimizing this cost function, the free parameters are optimized in order to attain an energy efficient locomotion when the tracking performance is not very important. For instance, humans do not have a precise motion control during walking, and only some important states should be met; i.e., toe-off and heel-strike. Similar to Eqs. (14), (15) cannot be solved by classic analytical optimization algorithms and we use GA to solve this optimization. Nevertheless, in Smit-Anseeuw, Gleason, Vasudevan, and Remy (2017), another optimization algorithm is suggested for resolving the optimization problems based on COT.

3.5. Energy consumption of impulsive actuation

In this subsection, we derive a lower bound for energy consumption of *impulsive actuation* based on the change of stored energy in the series springs (K_s). Accordingly, the energy consumption in the ith interval is $E_{ci} = \sum_{j=1}^{n} |E_{aji} - E_{bji}|$, where $E_{bji}(E_{aji})$ is the energy of spring before(after) actuation instant at the jth joint. The absolute value is used here to indicate that the actuation system cannot recycle the negative work. For computing E_c in terms of q_s, we can replace $E_{bji}(E_{aji})$ with the stored energy in the serial spring before(after) the actuation instants as:

$$E_c = \sum_{i=1}^{N_r} \sum_{j=1}^{n} \| \underbrace{0.5K_s(q_{ji} - q'_{sji})^2}_{E_{aji}} - \underbrace{0.5K_s(q_{ji} - q''_{sji})^2}_{E_{bji}} \|_2$$

where q_{ji} is the jth joint position, and $q''_{sji}(q'_{sji})$ is the actuator's shaft position before(after) the ith actuation instant.

3.6. Robustness analysis

Here, we study the robustness of the system in terms of boundedness of the tracking error in the face of noise in sensory feedback, disturbance, and perturbation.

As it can be seen in Fig. 1a, the presented controller is composed of two loops; called hereinafter as the inner and outer loops. The inner loop is responsible for guaranteeing the globally stability (see Section 3.1 for proof) using implemented compliances and dampers. It applies torque as a function of real joints' positions/velocities. Hence, it is immune to sensory noise. On the other hand, the outer loop which supervises the performance of the inner loop, applies an impulsive torque as a function of the desired joint position (Eq. (9)) at the transition phases based on the overall tracking error. Therefore, the sensory noise cannot penetrate this loop as well. The only parameter affected by noise is the tracking error and accordingly the decision-making process. In fact, increasing/decreasing the measured tracking error by adding noise in sensory feedback leads to increasing/decreasing the number of impulse actuations. Increasing the number of impulsive actuations may only increase the energy consumption but improves the tracking performance. If the added noise in feedback reduces the measured tracking error, it only disturbs the tracking performance since the stability is guaranteed by the inner loop. Moreover, the effect of noise can be moderated by reducing the decision boundary (ϵ). This may increase the number of actuations, but improves the robustness against the noise in sensory feedback and prevents tracking error amplification.

In the robotic field, the external disturbances/perturbations are mainly caused by external effects (e.g., obstacles) and modeled as additive forces/torques in the dynamical equations. It is generally accepted that using SEAs add intrinsic robustness to the system and improves the stability (Niehues, Rao, & Deshpande, 2015). For instance, in legged locomotion, having a compliant leg increases the mechanical stability margins; this feature is named as self-stability and introduced in Blickhan et al. (2007). Moreover, SEAs act as a filter and moderate the effects of collision with an obstacle; this behavior in face of external disturbances is named as safety (Tonietti, Schiavi,

& Bicchi, 2005). Interestingly, our presented method mostly utilizes the compliances and dampers to control the system and the impulsive actuations are applied through SEAs. As a conclusion, based on the mathematics presented in Section 3.1 and the pieces of evidence from literature, we can claim that the presented method is robust in the face of external disturbances/perturbations. In other words, if external disturbances/perturbations do not force the system to violate the stability conditions (presented in Section 3.1), the system remains stable. Furthermore, perturbations which are known and are functions of position, can be easily rejected by a proper compliance design, since the compliance is also a function of the position.

4. Simulations

Here, we verify the applicability of our method in three different case studies. The first one is the task of throwing an object by a 2-link arm, performing an explosive task. The second one is a 2-DOF manipulator representing the swing leg, performing a cyclic task. And the third one is a 3D quadruped robot which is one of the most complicated systems in sense of classic control. By means of these examples, we not only investigate the applicability of our method for different robotic purposes but also provide examples for the three presented cost functions in Section 3.4.

4.1. 2-link arm

Consider the task of throwing an object[3] by a 2-link arm towards a target shown in Fig. 3a. This 2-link planar manipulator could be thought of as a simplified model for a human arm as in Braun, Howard, and Vijayakumar (2012) and Ichinose, Katsumata, Nakaura, and Sampei (2008). At the beginning, the end-effector of the robot is initialized at state[4] 'A'. Through designing passive elements for the joints of this robot, we aim to throw the object at state 'B' towards the target (point 'G'). Here, in order to utilize the approach, we redefine this task of dynamic manipulation by considering an additional state 'C' as the equilibrium state for the robot to converge to; i.e., 'C' is the desired equilibrium point and $(q_C, \dot{q}_C) = (q_d, 0)$. Needless to say that, the path along which the end-effector moves from state 'A' to 'C', passes through state 'B'. Thus, we consider the following parameters for the task.

$$(x, y)_G = (4\text{ m}, 2\text{ m}) \quad , \quad (x, y)_B = (0\text{ m}, 1.5\text{ m})$$

In order to make the problem solvable (equal number of equations and unknowns), we also assume that the collision point (point 'G') is at the apex of the ballistic motion. Therefore, initial velocity from the release state ('B') as well as collision time is calculated as $(\dot{x}, \dot{y})_B = (12.53\text{ m/s}, 3.13\text{ m/s})$ and $t_c = 0.32$ s, respectively. Also joint positions and velocities at the release position are:

$$q_B = \begin{bmatrix} 48.59 & 82.82 \end{bmatrix}^T \text{(Deg)}$$
$$\dot{q}_B = \begin{bmatrix} -342.89 & -271.31 \end{bmatrix}^T \text{(Deg/s)}.$$

Since it is the release state that guarantees the object to reach the target, we define the starting and ending states of the manipulator arbitrary, yet feasible to fulfill the task.

$$q_A = \begin{bmatrix} 120 & 120 \end{bmatrix}^T \text{(Deg)} \, , \, \dot{q}_A = \begin{bmatrix} 0 & 0 \end{bmatrix}^T \text{(Deg/s)}$$
$$q_C = \begin{bmatrix} 30 & 22.5 \end{bmatrix}^T \text{(Deg)} \, , \, \dot{q}_C = \begin{bmatrix} 0 & 0 \end{bmatrix}^T \text{(Deg/s)}$$

Now, using the optimization stated in Section 3.4 with Eq. (13) as the cost function, we intend to calculate the passive elements for this robot such that once the robot is initialized at state 'A', passes through state 'B' and stops at 'C'; and $q_d = q_C$. Note that the foregoing optimization is defined over the trajectory of the system, whereas in this example only three states on the trajectory need to be followed. Thus, the optimization is redefined as follows.

$$(K_{opt}, B_{opt}) = arg \min_{K,B} \sum_{i=A,B,C} H_{ir}^{*T} H_{ir}^{*}$$

Minimization of this cost function is obtained once $H_{ir}^{*} = 0$ for all states. By considering all the constraints in Eq. (12), $F_d = F_{cC} + G_C$ is obtained as a function of compliance coefficients and $H_{Cr}^{*} = 0$ is guaranteed. Also, to have $H_{Ar}^{*} = H_{Br}^{*} = 0$, substituting states 'A', 'B' and F_d in Eq. (7) yields the following equations.[5]

$$M_A \ddot{q}_A + G_A + F_{cA} - F_{cC} - G_C = 0$$
$$M_B \ddot{q}_B + C_B \dot{q}_B + G_B + F_{cB} + F_{bB} - F_{cC} - G_C = 0$$

Here, the linear basis function is considered for both the compliance and the damper profiles. Now, computing the coefficients of compliance and damper is just a matter of finding $\ddot{q}_A$ and $\ddot{q}_B$. For that, we employed a genetic algorithm. Having these accelerations, the compliances and dampers in each joint are easily obtained as follows.

$$K = [\ 1393.50 \quad 237.77]^T \text{ (Nm/rad)}$$
$$B = [\ 97.58 \quad 65.45]^T \text{ (Nm s/rad)}$$

Fig. 4a–d shows the end-effector's position, end-effector's horizontal and vertical velocities, joints' angles, and joints' angular velocities. It can be seen that the end-effector passes through state 'B' with desired velocities once it is initialized at state 'A'.

4.2. Swing leg

Consider a two-link planar manipulator acting as a swing leg; see Fig. 3b. Here, the end-effector's task is to perform an oval-shaped motion with radius of $(r_x, r_y) = (0.4, 0.2)$ m, centered at $(x, y) = (0, -1.7)$ m, and frequency equal to $\omega = 5$ rad/s. In this simulation the decision boundary for the outer loop is set to $\epsilon = 0.1$.

The control law discussed in Section 3.3 is utilized for performing the cyclic task smoothly. Here, the value of F_d required for transition between phases is computed according to Eq. (9) for each interval. Also, compliances and dampers for each joint are obtained through minimizing Eq. (14) with $\lambda(t) \equiv 0$ and $\beta(t) \equiv 1$ by a GA.[6] The rounded results are:

1. Nonlinear compliance coefficients: $(\phi = [q \ , \ q^3]^T)$
   First joint: $k_{11} = 20\ \frac{\text{Nm}}{\text{rad}}, k_{12} = -15\ \frac{\text{Nm}}{\text{rad}^3}$
   Second joint: $k_{21} = 5\ \frac{\text{Nm}}{\text{rad}}, k_{22} = -15\ \frac{\text{Nm}}{\text{rad}^3}$.
2. Linear damper coefficients: $(\psi = \dot{q})$
   First joint: $b_{11} = 6\ \frac{\text{Nm s}}{\text{rad}}$
   Second joint: $b_{21} = 1\ \frac{\text{Nm s}}{\text{rad}}$.

The results obtained from this simulation are illustrated in Fig. 4e–h. As can be seen from Figs. 4e and 4f, the task is accomplished at the cost of tolerating some minor errors. These errors can be decreased by increasing the number of control intervals; see Fig. 4h. Fig. 4g shows the controller commands (F_d) required for this tracking performance; i.e., the changes in the precompression (F_d) of serial spring at each joint.

To test the robustness/performance of the system both in face of the noise and disturbance, we consider two different scenarios. In the first scenario, we have sensory noise in power of 10 and an additive time-vanishing-disturbance. The disturbance is a single square pulse which starts at $t = 5$ s and finishes at $t = 6$ s with the amplitude

[3] To avoid adding any further complexity in this simulation and without loss of generality, we assume that the object mass is negligible compared to the robot. Hence, it is not added to dynamical equations of the robot.

[4] Here, states 'A', 'B', and 'C' refer to both positions and velocities of the 2-link arm at configurations 'A', 'B', and 'C', respectively; see Fig. 3a.

[5] M_i indicates the value of mass matrix in state 'i'.

[6] It is important to note that by setting $\lambda(t) \equiv 0$ and $\beta(t) \equiv 1$, the cost function, Eq. (14), presents the square of RMS tracking error.

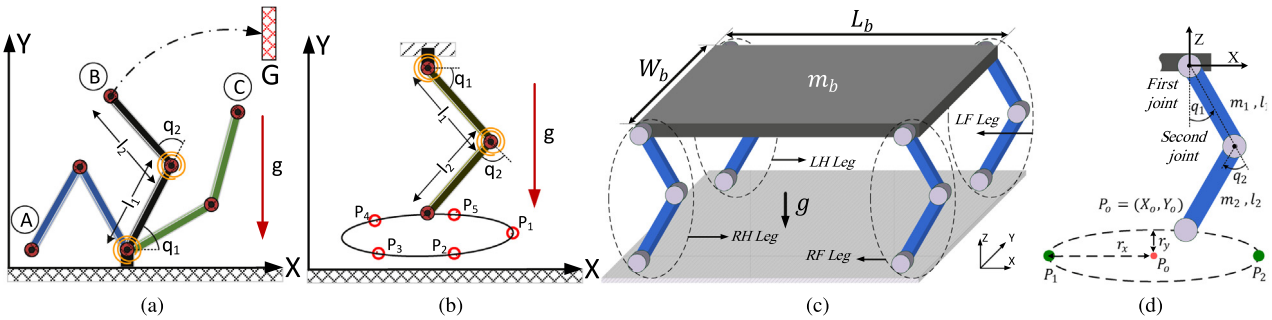

Fig. 3. Simulation models. (a): Schematic of 2-link arm throwing an object at release state 'B' to 'G'. (b): 2-DOF swing leg performing the cyclic task of walking. In both simulations, the links' parameters are considered as $m_i = 1$ kg , $L_i = 1$ m $\forall i \in \{1, 2\}$. (c,d): Schematic of a 3D model of quadruped robot with point feet and soft impact model. The mass of the body and the first and the second link in each leg are $m_b = 12$ kg, $m_1 = 5$ kg, and $m_2 = 2$ kg, respectively. In addition, dimensions of the robot are set to $W_b = 1$ m, $L_b = 1.5$ m, $l_1 = 52$ cm, and $l_2 = 40$ cm so as to reach a model similar to quadrupeds. In all of the models, the gravity acceleration is $g = 9.81$ m/s^2.

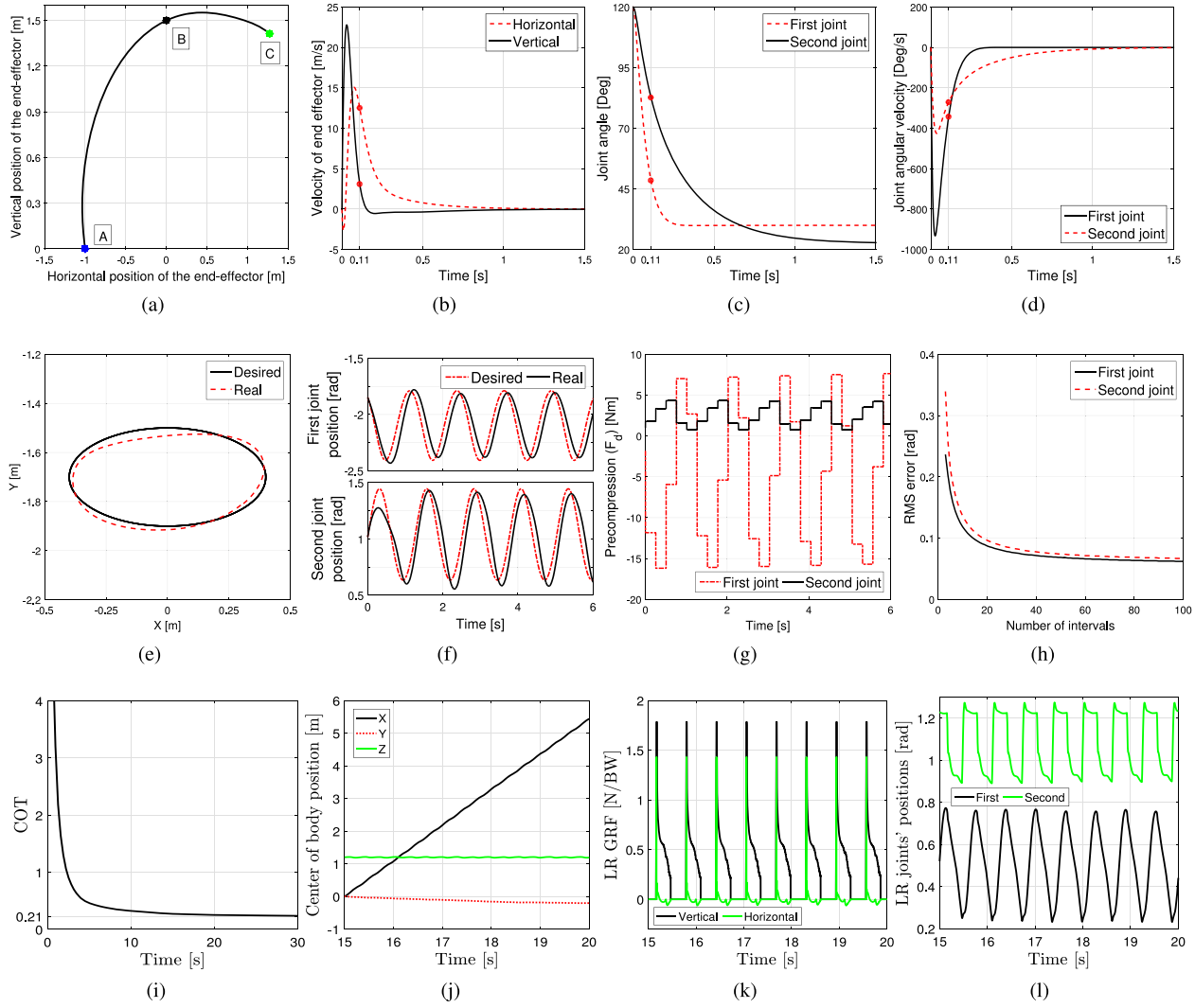

Fig. 4. (a–d): Simulation results of the 2-Link arm throwing an object towards a target: (a) shows the end-effector's trajectory. It can clearly be seen that at time $t = 0.11$ s, the robot is in the release configuration and the requirement $(\dot{x}, \dot{y})_B = (12.53 \text{ m/s}, 3.13 \text{ m/s})$ is met. (b) illustrates the horizontal and vertical velocities of the end-effector. (c) illustrates the evolution and convergence of the joint positions to their respective desired equilibrium points and (d) shows the angular velocity of both joints. (e–h): Simulation results of 2-DOF swing-leg model performing a cyclic task. For performing this task, the oval (i.e., path) is divided into five subtasks located at certain positions on the oval with phase shift equal to $2\pi/5$. (e) shows the end-effector's trajectory. Figure (f) illustrates the first and the second joint positions. (g) represents the changes in the serial spring's precompression at actuation intervals. And (h) shows how, by increasing the number of intervals, the RMS tracking error is minimized. (i–l): Simulation results for the quadruped robot. (i) shows the *COT* of quadruped robot in course of walking. (j) displays the center of body position. (k) presents GRFs of soft impact model during walking, which is normalized by body weight (BW). (l) depicts the joints' positions. The last three sub-figures (j–l) are plotted in the steady state condition after 15 s from the beginning of simulation.

of 10 N m. The second scenario has a non-vanishing-disturbance and a sensory noise in power of 10. Non-vanishing-disturbance is a pulse train with a period of 2 s, pulse-width of 50%, and amplitude of 5 N m. The results for both scenarios are presented in Fig. 5. As it can be seen

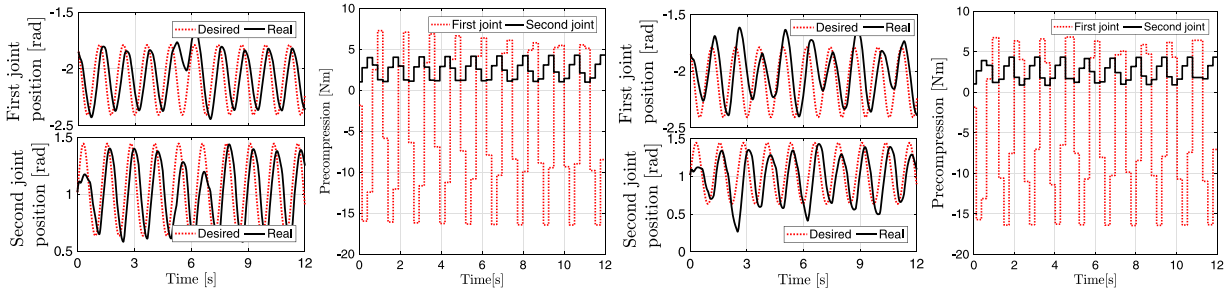

Fig. 5. Simulation for analyzing the performance of the controller in the face of noise in the sensory feedback and additive vanishing and non-vanishing perturbations. (a–b) are the position and precompression in presence of sensory noise with power of 10 and an additive vanishing perturbation starts at $t = 5$ s and finishes at $t = 6$ s with amplitude of 10 N m. In addition, (c–d) are the position and precompression in presence of sensory noise with power of 10 and a non-vanishing additive perturbation as impulsive train with period of 2 s, pulse-width of 50%, and amplitude of 5 N m. As it can be seen in both of the scenarios the system remains stable.

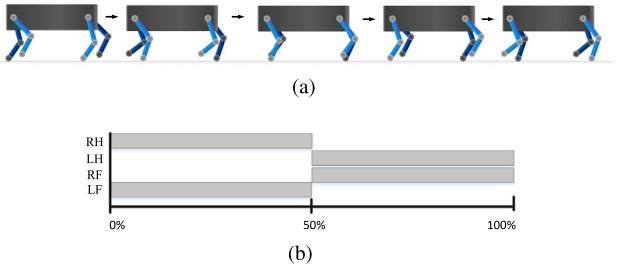

Fig. 6. (a) Snapshots of the quadruped walking in simulation environment, and (b) shows the gait pattern.

in Figs. 5a and 5b, after $t = 5$ s the vanishing disturbance disrupts the tracking error, however, after $t = 6$ s the tracking error improves. Moreover, Figs. 5c and 5d show the behavior of the system in face of a non-vanishing disturbance. Although the tracking error is bounded, the tracking performance is not desired. The system experiences high tracking errors, but it remains stable.

4.3. Quadruped robot

In order to show the applicability and robustness of the presented approach for control of robotic systems which their dynamical equations are not governed by Eq. (1), here, we apply our method on a 3D quadruped robot illustrated in Fig. 3c–d, which can move in the sagittal plane and perform the 2D tasks. By carrying out this simulation, we also aim to check if the presented method is capable of dealing with external vanishing disturbances (e.g., ground impacts), and have a stable and energy efficient walking locomotion. In this simulation, we do not add any extra limitations, formulations, and constraints on the presented method. Only the considered approach for the control of a 2-DOF manipulator in Section 4.2 is extended for a quadruped robot. However, the compliance and damper parameters are optimized for the quadruped robot while it is walking and facing with ground impacts. By doing so, we show that our simple control strategy is sufficient to achieve an optimal/stable walking behavior. The underactuated robot considered here has 14 DOFs with 8 actuators, and it possess nonlinear hybrid dynamical equations. This complex dynamical system with high dimensional state-space ($[q\ \dot{q}] \in \mathbb{R}^{28}$), complicates applying classical control approaches such as hybrid-zero-dynamics (HZD (Sreenath, Park, Poulakakis, & Grizzle, 2011)). To model the ground reaction force (GRF) of each leg, we have utilized the soft impact model presented in Geyer and Herr (2010). In addition, Eq. (15) is chosen as the cost function. Here, the goal is to achieve the trotting gait of the horse with $COT \approxeq 0.2$.

In order to create a stable walking gait, similar to cursorial animals, the robot is actuated only in two intervals, one at the toe-off instant (P_1) and the other at the heel-strike (P_2); see Fig. 3d. Each leg traverses an oval trajectory with radius, center, and frequency equal to $(r_x, r_y) = (15, 5)$ cm, $P_o = (0, -80)$ cm, and $\omega = 10$ rad/s, respectively. Also, a phase difference of 180 degrees is made between the diagonal leg pairs; see Fig. 6 for the gait pattern and duty cycle of each leg. To facilitate the optimization process, the compliance and damper forces are considered equal for all legs. Also, the value of F_d is considered the same for all of the legs, however, it is applied with different time shifts. The optimized parameters of the model, by minimization of COT with a GA, are as follows.

1. Nonlinear compliance coefficients: $(\phi = [q\ ,\ q^3]^T)$
   First joint: $k_{11} = 90\ \frac{\text{Nm}}{\text{rad}}, k_{12} = 63\ \frac{\text{Nm}}{\text{rad}^3}$
   Second joint: $k_{21} = 95\ \frac{\text{Nm}}{\text{rad}}, k_{22} = 63\ \frac{\text{Nm}}{\text{rad}^3}$.
2. Linear damper coefficients: $(\psi = \dot{q})$
   First joint: $b_{11} = 4\ \frac{\text{Nm s}}{\text{rad}}$
   Second joint: $b_{21} = 6.5\ \frac{\text{Nm s}}{\text{rad}}$.

Simulation results are presented in Fig. 4i–l. Fig. 4i shows the COT of the quadruped robot in course of motion. As it can be seen, the COT reaches to 0.21 in steady states which is comparable to that of horses according to Kuo (2007). Due to the similarity between figures and for avoiding redundant information, only the results of the LR leg are presented; other legs have similar graphs with a time-shift. Fig. 4j shows the center of body position in three different directions. As it is clear, the robot has a smooth locomotion with constant forward velocity (1.1 m/s). Fig. 4k displays the GRFs of the LR leg in the horizontal and the vertical directions. It can be seen that the no-sliding condition is satisfied by a friction coefficient[7] greater than 0.8. Finally, Fig. 4l illustrates the first and the second joints' positions of the LR leg at the steady state condition. According to this figure, it can be inferred that using the presented method, one can control the robot on smooth joint trajectories with periodic/stable behaviors. Since there are only two actuation intervals, F_d is a simple squared wave.

To check the robustness of the system in face of changes in compliance and damper parameters, we vary the parameters by ±20% and present COT and stability condition of the robot in Table 1. In this table, the instabilities are mechanical in which the robot is fallen-down. According to Table 1, the results show that the control approach has an overall robustness against the changes in the compliance and damper parameters. Moreover, by comparing the rows of Table 1, it is concluded that COT (cost function) is semi-quadratic w.r.t. the compliance coefficients, but COT is non-quadratic w.r.t. the damper coefficients. In addition, it can be seen that by fine-tuning the controller parameters, lower COTs can also be achieved; e.g., $COT = 0.0996$. However, our goal is to reach the COT of horses. Furthermore, it can be

[7] The minimum friction constant (μ_{min}) for no-sliding locomotion is the maximum value of the horizontal GRF divided by the vertical GRF.

Table 1
Analyzing the stability of quadruped robot in face of $\alpha\%$ changes in compliance and damper parameters. The numbers are COT of the robot in steady behavior. In each row only the considered parameter is changed and the others are fixed and equal to the values presented in Section 4.3.

	−20%	−15%	−10%	−5%	0%	5%	10%	15%	20%
k_{11}	unstable	unstable	0.4562	0.1674	0.2133	0.3763	0.5821	0.7696	0.9532
k_{12}	unstable	unstable	unstable	0.1887	0.2133	0.2280	0.2471	0.2747	0.3033
k_{21}	unstable	unstable	unstable	unstable	0.2133	0.2579	03220	0.3945	0.4678
k_{22}	unstable	unstable	unstable	0.4640	0.2133	0.2260	0.5524	0.9605	1.3459
b_{11}	0.1816	0.1622	0.0996	0.2177	0.2133	0.2150	0.2015	0.2017	0.1762
b_{21}	0.2015	0.2035	0.2080	unstable	0.2133	0.2156	unstable	unstable	unstable

seen that for the compliance coefficients, the optimal points are close to instability boundaries, which is an interesting observation similar to animal strategy in locomotion. Animals approach mechanical-instability boundaries to increase their efficiency especially in higher speeds; e.g., sprint running (Romanov & Fletcher, 2007).

5. Discussions & conclusions

In this paper, inspired from pieces of biological evidence on legged animals, we presented a mathematical framework for impulsive control of robotic systems with cyclic and explosive tasks by means of designing passive elements; i.e., compliance and damper. In doing so, we presented a new perspective to control the robotic systems. And, accordingly, two new concepts were analytically defined: *passive internal controller* (PIC) and *impulsive actuation*. The PIC is the force of the passive elements considered as nonlinear state feedbacks and utilized for natural dynamics modification. And, the *impulsive actuation* is the force effect of a SEA system with fast action dynamic which is used for energy injection and preventing deviations from the desired trajectory.

We showed analytically that for explosive tasks the PIC guarantees a globally asymptotically stable convergence to the desired configuration. This approach was then extended to include periodic tasks. For that, a given cyclic task was regarded as a series of explosive subtasks and thereafter each of these newly formed subtasks was performed by the same proposed method. Transition between these aperiodic phases was also done with the *impulsive actuation*. It is noteworthy to mention that by investing more on the modification of natural dynamics (i.e., developing the PIC) rather than directly actuating the system, fewer time intervals are required and ergo, lesser energy is consumed.

In this approach, we have redundancy in selecting the compliance and damper parameters. Hence, in addition to control the robot towards the actuation intervals, an optimization problem can also be solved to attain other objectives such as minimizing tracking error or increasing energy efficiency. Moreover, we studied the robustness of our method in face of uncertainties and disturbances and discussed that the presented control framework can handle them effectively; thus, it is applicable for real-world systems.

Three examples were presented to investigate the applicability of our method in robotics: a 2-link arm, a swing leg, and a 3D quadruped robot. The results obtained from simulating these case studies demonstrated the effectiveness and notable benefits of employing our approach both in manipulators and legged robots. More specifically, achieving a COT of 0.21 comparable to horses is an interesting finding of simulating the 3D quadruped robot. And it indicates the potential of the presented method for improving the performance of robotic systems and even modeling the behavior of biological systems. Accordingly, our method can widely be used in different robotic systems to improve their performance (in terms of efficiency, robustness, and controllability) by reducing the complexity of control strategies and granting intrinsic robustness; i.e., self stability.

From the practical point of view, by means of the presented strategy, the actuators remain off until the *impulsive actuation* is required. Hence, at each actuation interval, they apply torque at the starting condition. In dc-motors, the starting torque is much more than the nominal one. Hence, for a certain amount of torque, smaller and lighter dc-motors can be utilized. Consequently, the total mass of legged robots is reduced, which significantly improves their efficiency.

These shreds of evidence form simulations, mathematics, and literature review, ensure the effectiveness of impulsive actuation system. But still no hardware is developed for realization of this concept. As for the future work, we are going to develop a mechanism for realization of impulsive actuation concept and experiment our method in real robotic systems.

Acknowledgment

Authors would like to thank University of Tehran for providing support for this work.

Conflict of interest

None declared.

References

Aoustin, Y., Romero, D. T., Chevallereau, C., & Aubin, S. (2006). Impulsive control for a thirteen-link biped. In *Advanced motion control, 2006. 9th IEEE international workshop on* (pp. 439–444). IEEE.

Bhounsule, P. A., Ruina, A., & Stiesberg, G. (2015). Discrete-decision continuous-actuation control: balance of an inverted pendulum and pumping a pendulum swing. *Journal of Dynamic Systems, Measurement, and Control*, *137*(5), 051012.

Bidgoly, H. J., Ahmadabadi, M. N., & Zakerzadeh, M. R. (2016). Design and modeling of a compact rotational nonlinear spring. In *Intelligent robots and systems (IROS), 2016 IEEE/RSJ international conference on* (pp. 4356–4361). IEEE.

Biewener, A. A., & Roberts, T. J. (2000). Muscle and tendon contributions to force, work, and elastic energy savings: a comparative perspective. *Exercises Sport Science Reviews*, *28*(3), 99–107.

Blickhan, R., Seyfarth, A., Geyer, H., Grimmer, S., Wagner, H., & Günther, M. (2007). Intelligence by mechanics. *Philosophical Transactions of the Royal Society of London A: Mathematical, Physical and Engineering Sciences*, *365*(1850), 199–220.

Braun, D. J., Howard, M., & Vijayakumar, S. (2012). Exploiting variable stiffness in explosive movement tasks. *Robotics: Science and Systems*, *VII*, 25.

von Brecht, C., Kramer, B., Bhounsule, P., & Jafari, A. (2016). An impulse actuator for high speed & high torque applications. *Dynamic Walking*, 4–7.

Byl, K., & Tedrake, R. (2008). Approximate optimal control of the compass gait on rough terrain. In *Robotics and automation, 2008. ICRA 2008. IEEE international conference on* (pp. 1258–1263). IEEE.

Caputo, J. M., & Collins, S. H. (2014). Prosthetic ankle push-off work reduces metabolic rate but not collision work in non-amputee walking. *Scientific Reports*, *4*, 7213.

Choi, J. H., & Grizzle, J. (2005). Feedback control of an underactuated planar bipedal robot with impulsive foot action. *Robotica*, *23*(05), 567–580.

Collins, S., Ruina, A., Tedrake, R., & Wisse, M. (2005). Efficient bipedal robots based on passive-dynamic walkers. *Science*, *307*(5712), 1082–1085.

Dickinson, M. H., Farley, C. T., Full, R. J., Koehl, M., Kram, R., & Lehman, S. (2000). How animals move: an integrative view. *science*, *288*(5463), 100–106.

Formalskii, A. M. (2009). Ballistic walking design via impulsive control. *Journal of Aerospace Engineering*, *23*(2), 129–138.

Geyer, H., & Herr, H. (2010). A muscle-reflex model that encodes principles of legged mechanics produces human walking dynamics and muscle activities. *IEEE Transactions on neural systems and rehabilitation engineering*, *18*(3), 263–273.

Giardina, F., & Iida, F. (2018). Efficient and stable locomotion for impulse-actuated robots using strictly convex foot shapes. *IEEE Transactions on Robotics*, *1*(1), 1–8.

Haldane, D. W., Plecnik, M., Yim, J. K., & Fearing, R. S. (2016). Robotic vertical jumping agility via series-elastic power modulation. *Science Robotics*, *1*(1), 1–8.

Hill, A. V. (1938). The heat of shortening and the dynamic constants of muscle. *Proceedings of the Royal Society of London. Series B-Biological Sciences*, *126*(843), 136–195.
Ichinose, S., Katsumata, S., Nakaura, S., & Sampei, M. (2008). Throwing motion control experiment utilizing 2-link arm passive joint. In *SICE annual conference, vol. 2008* (pp. 3256–3261). IEEE.
Khalil, H. K. (2002). *Nonlinear systems*. Prentice Hall Upper Saddle River.
Khoramshahi, M., Parsa, A., Ijspeert, M., & Nili Ahmadabadi, Auke (2014). Natural dynamics modification for energy efficiency, a data driven parallel compliance design method. In *International conference on robotics and automation (ICRA). Vol. 2014*.
Kim, B., & Deshpande, A. D. (2014). Design of nonlinear rotational stiffness using a noncircular pulley-spring mechanism. *Journal of Mechanisms and Robotics*, *6*(4), 041009.
Kuo, A. D. (2002). Energetics of actively powered locomotion using the simplest walking model. *Journal of Biomechanical Engineering*, *124*(1), 113–120.
Kuo, A. D. (2007). Choosing your steps carefully. *IEEE Robotics & Automation Magazine*, *14*(2), 18–29.
Mathis, F. B., Jafari, R., & Mukherjee, R. (2014). Impulsive actuation in robot manipulators: Experimental verification of pendubot swing-up. *IEEE/ASME Transactions on Mechatronics*, *19*(4), 1469–1474.
McGeer, T. (1993). Dynamics and control of bipedal locomotion. *Journal of Theoretical Biology*, *163*(3), 277–314.
Meinders, M., Gitter, A., & Czerniecki, J. M. (1998). The role of ankle plantar flexor muscle work during walking. *Scandinavian Journal of Rehabilitation Medicine*, *30*(1), 39–46.
Nasiri, R., Khoramshahi, M., Shushtari, M., & Ahmadabadi, M. N. (2016). Adaptation in variable parallel compliance: Towards energy efficiency in cyclic tasks. *IEEE/ASME Transactions on Mechatronics*, 1–12.
Niehues, T. D., Rao, P., & Deshpande, A. D. (2015). Compliance in parallel to actuators for improving stability of robotic hands during grasping and manipulation. *International Journal of Robotics Research*, *34*(3), 256–269.
Ott, C. (2008). *Cartesian impedance control of redundant and flexible-joint robots*. Springer.
Plooij, M., & Wisse, M. (2012). A novel spring mechanism to reduce energy consumption of robotic arms. In *2012 IEEE/RSJ international conference on intelligent robots and systems* (pp. 2901–2908). IEEE.
Romanov, N., & Fletcher, G. (2007). Runners do not push off the ground but fall forwards via a gravitational torque. *Sports Biomechanics*, *6*(3), 434–452.
Shushtari, M., Nasiri, R., Yazdanpanah, M. J., & Ahmadabadi, M. N. (2017). Compliance and frequency optimization for energy efficiency in cyclic tasks. *Robotica*, 1–18.
Smit-Anseeuw, N., Gleason, R., Vasudevan, R., & Remy, C. D. (2017). The energetic benefit of robotic gait selectiona case study on the robot ramone. *IEEE Robotics and Automation Letters*, *2*(2), 1124–1131.
Sreenath, K., Park, H.-W., Poulakakis, I., & Grizzle, J. W. (2011). A compliant hybrid zero dynamics controller for stable, efficient and fast bipedal walking on mabel. *International Journal of Robotics Research*, *30*(9), 1170–1193.
Srinivasan, M., & Ruina, A. (2006). Computer optimization of a minimal biped model discovers walking and running. *Nature*, *439*(7072), 72.
Tonietti, G., Schiavi, R., & Bicchi, A. (2005). Design and control of a variable stiffness actuator for safe and fast physical human/robot interaction. In *Robotics and automation, 2005. ICRA 2005. proceedings of the 2005 IEEE international conference on* (pp. 526–531). IEEE.
Verstraten, T., Beckerle, P., Furnémont, R., Mathijssen, G., Vanderborght, B., & Lefeber, D. (2016). Series and parallel elastic actuation: Impact of natural dynamics on power and energy consumption. *Mechanism and Machine Theory*, *102*, 232–246.
Wilson, A. M., Watson, J. C., & Lichtwark, G. A. (2003). Biomechanics: a catapult action for rapid limb protraction. *Nature*, *421*(6918), 35–36.
Zamani, A., & Bhounsule, P. A. (2017). Foot placement and ankle push-off control for the orbital stabilization of bipedal robots. In *Intelligent robots and systems (IROS), 2017 IEEE/RSJ international conference on* (pp. 4883–4888). IEEE.
Zelik, K. E., Huang, T.-W. P., Adamczyk, P. G., & Kuo, A. D. (2014). The role of series ankle elasticity in bipedal walking. *Journal of Theoretical Biology*, *346*, 75–85.

Rezvan Nasiri was born in December 1989. He received his B.S. degree in Electrical Engineering from University of Gilan in September 2012. He received M.Sc. in Control Engineering from University of Tehran under Prof. Nili and Prof. Yazdanpanah's supervision in September 2014. He is currently a Ph.D. candidate in Cognitive Robotic Laboratory under supervision of Prof. Nili at University of Tehran. His main research interests are bio-inspired design, legged locomotion, system dynamics, machine learning, rehabilitation, and bionic.

Armin Zare was born in August 1995. He received his B.S. degree in Imam Khomeini International University. He received M.Sc. in Control Engineering from University of Tehran under Prof. Nili's supervision in September 2017. His main research interests are legged robots and nonlinear dynamical systems.

Omid Mohseni received the B.Sc. degree in Electrical Engineering from Azad University, Karaj Branch, Iran in 2014, and the M.Sc. degree from University of Tehran, Iran in 2017. Since then he has been a research assistant in Cognitive Robotics Laboratory under the supervision of Prof. Majid Nili Ahmadabadi at University of Tehran. Currently, he is a visiting student in the Lauflabor Locomotion Laboratory at the Institute of Sports Science of the Technische Universität Darmstadt, under the supervision of Prof. Dr. Andre Seyfarth and Dr. Maziar Ahmad Sharbafi. His research interests focus on bio-inspired legged robots and locomotion, energy efficient actuation and control, and rehabilitation.

Mohammad Javad Yazdanpanah received the B.Sc., M.Sc., and Ph.D. degrees from Isfahan University of Technology, Isfahan, Iran, in 1986, the University of Tehran, Tehran, Iran, in 1988, and Concordia University, Montreal, QC, Canada, in 1997, respectively, all in electrical engineering. In 1998, he joined the School of Electrical and Computer Engineering, University of Tehran, where he is currently a Professor and Director of the Advanced Control Systems Laboratory. His research interests include analysis and design of nonlinear/optimal/adaptive control systems, robotics, control on networks, and theoretical and practical aspects of neural networks.

Majid Nili Ahmadabadi (M.N. Ahmadabadi) was born in 1967 and received his B.S from Sharif University of Technology of Iran in 1990. He received his M.Sc. and Ph.D. in Information Sciences from the Graduate School of Information Science, Tohoku University, Japan in 1994 and 1997 respectively. In 1997, he joined the Advanced Robotics Laboratory at Tohoku University. Later he moved to School of Electrical and Computer Engineering, College of Engineering, University of Tehran where he is a professor and the head of Robotics and AI Laboratory. Dr. Ahmadabadi is the founder and the director of Cognitive Systems Laboratory as well. He is also a senior researcher at School of Cognitive Sciences, Institute for Research in Fundamental Sciences (IPM), Iran. He was one of the distinguished lecturers selected by IEEE Robotics and Automation Society for the years 2007- 2009. Dr. Ahmadabadi served as a member of the engineering board of Iranian National Science Foundation for the period 2005-2011. He is one of the founders of The Robotics Society of Iran in addition to the Iranian Society of Cognitive Sciences. His main research interests are cognitive robotics and modeling cognitive systems in addition to control of legged robots.